Modeling electro-mechanical properties of layered electrets: Application of the finite-element method

Enis Tuncer,* Michael Wegener, Reimund Gerhard-Multhaupt

Applied Condensed-Matter Physics, Department of Physics, University of Potsdam, D-14469 Potsdam Germany

Abstract

We present calculations on the deformation of two- and three-layer electret systems. The electrical field is coupled with the stress-strain equations by means of *the Maxwell stress tensor*. In the simulations, two-phase systems are considered, and intrinsic relative dielectric permittivity and Young's modulus of the phases are altered. The numerically calculated electro-mechanical activity is compared to an analytical expression. Simulations are performed on two- and three-layer systems. Various parameters in the model are systematically varied and their influence on the resulting piezoelectricity is estimated. In three-layer systems with bipolar charge, the piezoelectric coefficients exhibit a strong dependence on the elastic moduli of the phases. However, with mono-polar charge, there is no significant piezoelectric effect. A two-dimensional simulation illustrated that higher piezoelectricity coefficients can be obtained for non-uniform surface charges and low Poisson's ratio of phases. Irregular structures considered exhibit low piezoelectric activity compared to two-layer structures.

Key words: Piezoelectricity and electro-mechanical effects, Layered electrets, Finite-element method

1 Introduction

Charged dielectric films with soft elastic properties and at least one free (unclamped) surface can be used as electro-mechanical and electro-acoustic

* Corresponding author.
Email address: enis.tuncer@physics.org (Enis Tuncer,).

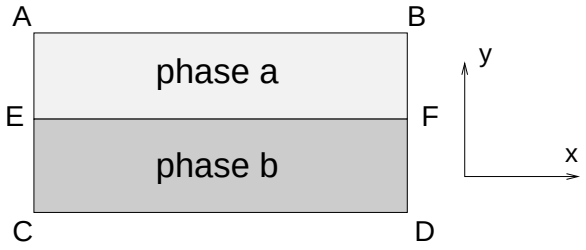

Fig. 1. Computation domain for the two-layer system.

transducers[1, 2]. Traditional materials for such applications have been inorganic crystalline substances[3]. The electro-mechanical effect (piezoelectricity) observed in organic polymeric materials differs in several aspects from that of traditional inorganic piezoelectric materials. Apart from morphological differences, piezoelectricity in polymers is based either on (i) oriented molecular dipoles (domains) or on (ii) trapped charges whose distribution breaks the symmetry inside the non-uniform anisotropic material. The underlying mechanisms of the phenomenological piezoelectricity in these materials have previously been presented in the literature[4, 5, 6, 7]. Recently, several potential candidates for large piezoelectric effects in heterogeneous or porous polymer systems are reported[8, 9, 10, 11, 12, 13, 14]. Although there exist analytical models for modeling simple geometries and uniform charge distributions, numerical solutions may be preferable for complex geometries[15, 16, 17] and non-uniform charge distributions. In this paper, the finite-element (FE) method is first applied to solve the electric field in two- and three-layered structures with interface, surface or volume charges. We have considered non-uniform charge distributions and irregular geometries as two-dimensional cases. The obtained electric field is later used in calculating the displacement vector by considering *the Maxwell stress tensor*. The results of the one-dimensional simulations illustrate that the use of *the Maxwell stress tensor* generates a perfect agreement with the analytical model. Since there are no analytical expressions for arbitrary geometries and structures with several materials and space-charge regions, the application of the FE method to such problems results in a better understanding of composite properties that may lead to new tailored materials.

2 Numerical Modeling

A model for the electro-mechanical response of a double-layer dielectric system with an interface charge ρ at the double-layer boundary has been presented by Kacprzyk et al. [6]. Layered systems have been shown as the optimal matrix microstructures for piezocomposites[18]. In the model, the dielectric and elastic properties of the phases a and b with thicknesses x_{a} and x_{b} are expressed with the high-frequency relative permittivities $\epsilon_{\mathsf{a,b}}$ and Young's moduli $E^{\mathrm{Y}}_{\mathsf{a,b}}$,

respectively. The piezoelectric coefficient for the composite system is then calculated as the ratio of the change of surface charge to the force applied perpendicular to the surface[6];

$$d_{33}^{\mathsf{e}} = -\frac{\rho\epsilon_{\mathsf{a}}\epsilon_{\mathsf{b}}x_{\mathsf{a}}x_{\mathsf{b}}(E_{\mathsf{a}}^{\mathrm{Y}} - E_{\mathsf{b}}^{\mathrm{Y}})}{E_{\mathsf{a}}^{\mathrm{Y}}E_{\mathsf{b}}^{\mathrm{Y}}(\epsilon_{\mathsf{b}}x_{\mathsf{a}} + \epsilon_{\mathsf{a}}x_{\mathsf{b}})^2} \tag{1}$$

Since there is no intrinsic piezoelectricity assumed in the phases, the coefficient d_{33} is written as an effective material property with a superscript 'e'. The term on the right-hand side of Eq. (1) containing permittivities is proportional to the effective dielectric permittivity of the system, $\epsilon^{\mathsf{e}} = \epsilon_{\mathsf{a}}\epsilon_{\mathsf{b}}(\epsilon_{\mathsf{b}}x_{\mathsf{a}} + \epsilon_{\mathsf{a}}x_{\mathsf{b}})^{-1}$. For complex structures, or layered systems with materials having different Poisson's ratios, Eq. (1) can not be applied.

Similarly, applying a numerical model, one should arrive at the same results. To this end, we have employed the FE method and performed simulations on a double-layer system. In the FE calculations, electrostatic field and stress-strain relations are solved simultaneously. Neglecting the polarization of the phases, the electric field $\mathbf{E}(= -\nabla\Phi(\mathbf{r}))$ distribution is obtained from Poisson's equation:

$$-\nabla \cdot [\varepsilon(\mathbf{r})\nabla\Phi(\mathbf{r})] = \rho(\mathbf{r}) \tag{2}$$

where Φ is the electric potential distribution, and ε and ρ are the dielectric permittivity ($\varepsilon = \epsilon\varepsilon_0$, ε_0 is the permittivity of free space and $\varepsilon_0 = 8.854$ pFm^{-1}) and the charge density as space-dependent variables, respectively. For the stress-strain relations, Navier's equation is solved,

$$-\nabla \cdot \mathbf{T}(\mathbf{r}) = \mathrm{K}(\mathbf{r}). \tag{3}$$

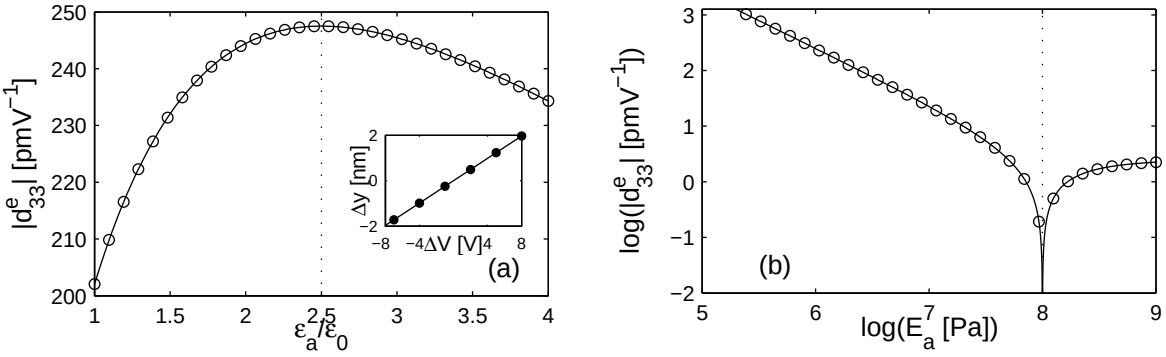

Fig. 2. Calculated piezoelectric coefficients d_{33}^{e} as a function of (a) the relative permittivity of phase a and (b) Young's modulus of phase a. The symbols ($\circ$) and the solid lines (——) represent the results of the FE calculations and the analytical expression of Eq. (1), respectively. The dotted ($\cdots\cdots$) lines represent the permittivity and Young's modulus of phase b, respectively. The inset in (a) illustrates the numerical results for $\varepsilon_{\mathsf{a}} = \varepsilon_{\mathsf{b}}$ for various voltages, the slope is the piezoelectric coefficient, 246 pmV^{-1}.

Here $\mathbf{T}$ and K are the stress tensor and the body force, respectively. The stress $\mathbf{T}$ is proportional to the gradient of the unknown displacement $\mathbf{u}(\mathbf{r})$ and the space-dependent material coefficient c, $\mathbf{T} = c\nabla\mathbf{u}$. The coefficient c is a function of Young's modulus E^{Y} and Poisson's ratio ν of the specific medium. The coupling of the electric field to the mechanical stress is achieved through *the Maxwell stress tensor*[19, 20].

$$\mathbf{T}'(\mathbf{r}) = c(\mathbf{r})\nabla\mathbf{u}(\mathbf{r}) - \frac{1}{2}\mathbf{D}(\mathbf{r})\cdot\mathbf{E}(\mathbf{r}) + \mathbf{E}(\mathbf{r})\mathbf{D}^{\mathrm{T}}(\mathbf{r}) \tag{4}$$

where $\mathbf{T}'$ is the generalized stress tensor. $\mathbf{E}$ and $\mathbf{D}$ are the electric field and the dielectric displacement vectors, and the superscript 'T' denotes a transposed matrix. The last term in Eq. (4) is the matrix direct product. Inserting (4) into the stress-strain relation of Eq. (3), the general equation for our calculations is obtained:

$$-\nabla\cdot[c(\mathbf{r})\nabla\mathbf{u}(\mathbf{r}) - \frac{1}{2}\mathbf{D}(\mathbf{r})\cdot\mathbf{E}(\mathbf{r}) + \mathbf{E}(\mathbf{r})\mathbf{D}^{\mathrm{T}}(\mathbf{r})] = \mathrm{K}(\mathbf{r}) \tag{5}$$

It is worth mentioning that the spatially varying material parameter ε and the charge distribution ρ in Eq. (2) are functions of the displacement $\mathbf{u}$[21, 22]. However, this coupling is not taken into consideration in this paper.

For layered structures and for one-dimensional simulations, the non-diagonal components in the last term on the left-hand side of Eq. (5) are neglected, and the Poisson's ratio ν of the materials in question is insignificant. No body-force term is considered in the simulations. In the following part, we solve Eqs. (2) and (5) with a nonlinear solver based on a commercially available FE software package[23]. First two- and three-layer systems with charge distribution(s) perpendicular to the applied field direction (in the y-direction) are considered; such a problem is pure one-dimensional. Later the charge distribution is considered to be non-uniform and again perpendicular to the applied field direction, which makes the problem two-dimensional. We have also assumed irregular two-dimensional structures in which the fraction of phase a is decreased in the layer.

3 Results and discussions

3.1 Two-layer system

An application of the numerical model to the geometrical conditions described by Kacprzyk et al. [6] confirmed that our approach is valid in one dimension with $\nu_{\mathsf{a,b}} \approx 0$ and $c = E^{\mathrm{Y}}$. In these simulations, the geometry for the computation is a layered structure with phases a and b, as shown in Fig. 1. The

two-layer system is a charged system that produces an external field which leads to piezoelectric properties[4].

The mechanical boundary conditions in the simulations are chosen such that the structure is fixed at CD, where it is not allowed to deform in the x- and y-directions. At the boundaries AB, AC and BD, the structure is allowed to move in the x- and y-directions. The voltage boundary conditions are applied at CD and AB with voltages V_{CD} and V_{AB}, and at AC and BD, symmetry conditions are assumed for the static electrical calculations, $\partial V/\partial x = 0$. Moreover, a surface charge density of $1\ \mathrm{mC\,m^{-2}}$ (attainable in experiments[8, 24]) is applied at the internal EF boundary. The thicknesses of the phases are taken equal to each other, $x_{\mathsf{a}} = x_{\mathsf{b}} = 1$ mm. The layer thickness in the simulations would not affect the overall effective properties of the mixture.

The electric-field-induced mechanical deformation Δy can be expressed as a power series. In that case, the electrostrictive a^{e}_{33} and piezoelectric d^{e}_{33} coefficients can be estimated from pairs of the position displacements at the boundary AB and the voltage difference between the AB and CD boundaries, $\Delta V = V_{\mathrm{AB}} - V_{\mathrm{CD}}$.

$$\begin{aligned}\Delta y &= y - y_0 \\ &= [d^{\mathsf{e}}_{33} + a^{\mathsf{e}}_{33}\Delta V + \dots]\,\Delta V\end{aligned} \tag{6}$$

where y_0 is the deformation without the voltage applied and due to the charge at the interface EF. We have adapted the first two terms of the series expansion at the right-hand-side of Eq. (6) in the numerical data analysis. The numerical results are shown as an inset in Fig. 2a. In the inset, the parameters y_0, d^{e}_{33} and a^{e}_{33} are 5.65×10^{-6} [m], 2.46×10^{-10} [pmV^{-1}] and -2.13×10^{-16}[pmV^{-2}], respectively. Observe that $a^{\mathsf{e}}_{33}\cdot\Delta V \ll d^{\mathsf{e}}_{33}$. The coefficients can be calculated with the following relations for the nonlinear, $a^{\mathsf{e}}_{33}\cdot\Delta V \gg d^{\mathsf{e}}_{33}$, and linear $d^{\mathsf{e}}_{33} \gg a^{\mathsf{e}}_{33}\cdot\Delta V$ regimes,

$$a^{\mathsf{e}}_{33} = \Delta y \Delta V^{-2} \quad [\mathrm{pmV^{-2}}] \tag{7}$$

$$d^{\mathsf{e}}_{33} = \Delta y \Delta V^{-1} \quad [\mathrm{pmV^{-1}}] \tag{8}$$

In Fig. 2, the simulation results and their comparison with Eq. (1) are presented. The permittivity and Young's modulus of phase b are kept constant, $\epsilon_{\mathsf{b}} = 2.5$ and $E^{\mathrm{Y}}_{\mathsf{b}} = 100$ MPa, respectively. First, the permittivity of phase a is varied between the free-space value ε_0 and $4\varepsilon_0$ while keeping Young's modulus of phase a constant, $E^{\mathrm{Y}}_{\mathsf{a}} = 1$ MPa. Then keeping the permittivity of phase a constant, $\epsilon_{\mathsf{a}} = 2.5$, Young's modulus of phase a is altered between 100 kPa and 1 GPa. These permittivity values are chosen, since most of the polymers have relative permittivities between 2 and 12. In addition, traditional ma-

terials containing voids (low-κ materials) usually have relative permittivities between 1 and 2. Young's moduli of the phases are on the other hand assigned on the basis of the effective medium theory[15] for layered structures and the measured effective moduli of porous polymers from Neugschwandtner et al. [24] and of some solid polymers from `MatWeb`[25].

The results are illustrated in Figs. 2a and 2b. In Fig. 2a, the effective piezoelectric coefficient $|d^{\mathsf{e}}_{33}|$ is plotted as a function of the relative permittivity of phase a permittivity. The symbols ($\circ$) and the solid line (——) represent the results of the FE calculations and the analytical expression Eq. (1), respectively. There is a maximum of $|d^{\mathsf{e}}_{33}|$ when the permittivities of the phases are equal to each other, $\epsilon_{\mathsf{a}} = \epsilon_{\mathsf{b}}$, which is also expected from Eq. (1). This indicates that one should tailor or choose materials with matching dielectric properties. In Fig. 2b the logarithm of $|d^{\mathsf{e}}_{33}|$ is displayed as a function of Young's modulus of phase a for $\epsilon_{\mathsf{a}} = \epsilon_{\mathsf{b}} = 2.5$. For a stiff phase a, $E^{\mathrm{Y}}_{\mathsf{a}} > E^{\mathrm{Y}}_{\mathsf{b}}$, d^{e}_{33} converges to a constant value. As $E^{\mathrm{Y}}_{\mathsf{a}}$ matches the value of $E^{\mathrm{Y}}_{\mathsf{b}}$, $E^{\mathrm{Y}}_{\mathsf{a}} \approx E^{\mathrm{Y}}_{\mathsf{b}}$ there is no piezoelectric activity, $\log(E^{\mathrm{Y}}_{\mathsf{a}}) = 8$. As the stiffness of phase a becomes lower than that of phase b, $|d^{\mathsf{e}}_{33}|$ increases. For $E^{\mathrm{Y}}_{\mathsf{a}} \ll E^{\mathrm{Y}}_{\mathsf{b}}$ there is a linear relation between $E^{\mathrm{Y}}_{\mathsf{a}}$ and $|d^{\mathsf{e}}_{33}|$ in the log-log graphs. The simulation indicate that there are are no nonlinear effects of the applied voltage on the deformation in these two-layer simulations, so that $a^{\mathsf{e}}_{33} \approx 0$ in Eq. (6), see inset in Fig. 2a. All these observation are also expected from Eq. (1), which is also presented in the figures with solid lines (——).

Next, we examine the influence of the charge distribution at the interface on d^{e}_{33}. To this end we introduce a volume charge distribution $\rho(x, y)$ which is only varied in the y-direction. The validity of Eq. (1) for such cases is discussed below. The charge distribution is generated with a delta sequence [26],

$$\phi_n(y) = n\pi^{-1}[1 + n^2y^2]^{-1} \tag{9}$$

where

$$\lim_{n\to\infty} \int \phi_n(y)\mathrm{d}y = 1.$$

In Eq. (9), n is a shape parameter. For charge distributions in the form of

$$\rho(x, y) = \rho_0\phi_n(y);$$

the volume charge distribution becomes surface charge distribution $\rho = \rho_0\delta(y)$ as $n \to \infty$.

In Fig. 3a the calculated $|d^{e}_{33}|$ is presented as normalized with the volume charge density ρ_0/Q_n for different shape parameters n, where

$$Q_n = \int \rho_0 \cdot \phi_n(y)\mathrm{d}y.$$

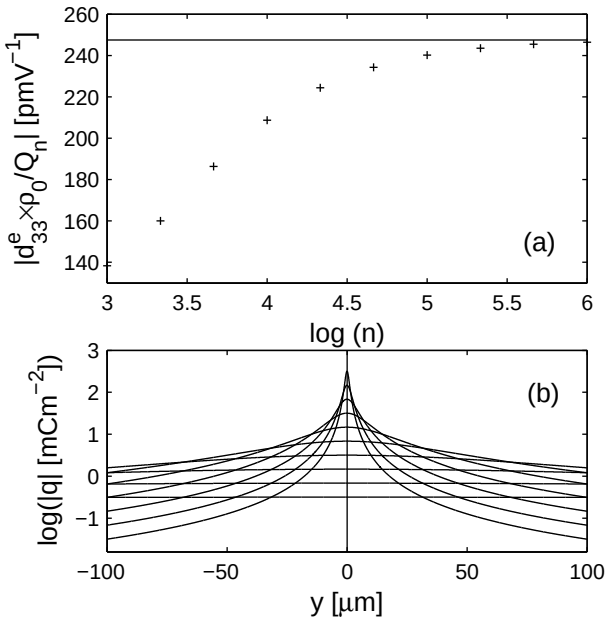

Fig. 3. (a) Calculated absolute values of piezoelectric coefficient $|d^e_{33}|$ normalized to the actual delta surface charge density ρ_0 and the total assumed volume charge density $Q_n = \int \rho(y)\mathrm{d}y$. The symbols (+) are results from the FE calculations, the solid line (——) represents the actual value from Eq. (1), $|d^e_{33}| = 247.5$ pmV^{-1} for a charge sheet. (b) Charge density distributions at the interface for $3 \leq n \leq 6$ in Eq. (9.

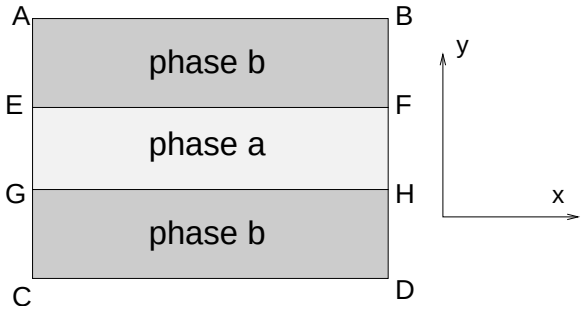

Fig. 4. Computation domain for the three-layer system.

The total volume charge density is not equal to ρ_0 because of the finite n. However, as n gets closer to 10^6, Eq. (9) can be used to represent a charge sheet. In Fig. 3b volume charge distributions are illustrated for the values of n used to calculate d^e_{33} in Fig. 3a. As the charge penetrates inside the material, forming a true space charge, the piezoelectric response of the composite system becomes weaker compared to a uniform sheet-like surface charge distribution.

Table 1
Minimum and maximum values of the parameters used in Eqs (6) for various simulations. Order means the layer sequence, soft-rigid-soft (SRS) and rigid-soft-rigid (RSR). The parameters varied in the simulations are also presented.

Order/	a_{33}^{e} [fmV^{-2}]		d_{33}^{e} [mV^{-1}]		y_0 [μm]	
Parameter	min	max	min	max	min	max
			Two-layer system			
——/ϵ_{a}			204p	250p	4.72	5.70
——/$E_{\mathsf{a}}^{\mathrm{Y}}$			−2.00p	2.49n	0.07	56.5
			bipolar charge system			
RSR/ϵ_{a}	2.27	2.79	−13.9f	−11.4f	0.23	0.25
SRS/ϵ_{a}	2.27	2.80	−245p	−200p	4.66	5.61
RSR/$E_{\mathsf{a}}^{\mathrm{Y}}$	0.03	27.7	−2.47n	2.20p	0.06	55.5
SRS/$E_{\mathsf{a}}^{\mathrm{Y}}$	0.03	27.7	−2.20p	2.47n	0.06	55.5
			mono-polar charge system			
RSR/ϵ_{a}	2.27	2.79	11.3f	14.0f	13.98	55.9
SRS/ϵ_{a}	2.27	2.79	−13.9f	−11.4f	0.23	0.25
RSR/$E_{\mathsf{a}}^{\mathrm{Y}}$	0.03	27.5	−0.13f	0.15p	0.02	223.7
SRS/$E_{\mathsf{a}}^{\mathrm{Y}}$	0.03	27.7	0.14p	0.13f	0.02	0.32

3.2 Three-layer systems

In order to enhance the efficiency of an electro-mechanical transducer, it is possible to stack layers of different materials. Such a system can be the three-layer binary structure ('a sandwich') which allows to employ and investigate different charge polarities. We therefore apply the numerical method to a three-layer binary system as shown in Fig. 4. In these simulations, (i) bipolar and (ii) mono-polar charge systems are assumed. In a bipolar system, the charge polarities at interfaces EF and GH in Fig. 4 are opposite to each other. In a mono-polar system, on the other hand, they have the same polarity. (The main difference between bi- and mono-polar charge systems is that bipolar charge systems do not contain unbalanced internal charge). The deformations Δy are analyzed as functions of the applied voltage difference $V_{\mathrm{AB}} - V_{\mathrm{CD}}$ with Eq. (6). The deformation Δy of a bipolar charge system is dominated by the contribution of the linear term, d_{33}^{e}. The deformation of a mono-polar charge system, on the other hand, shows negligible linear dependence and

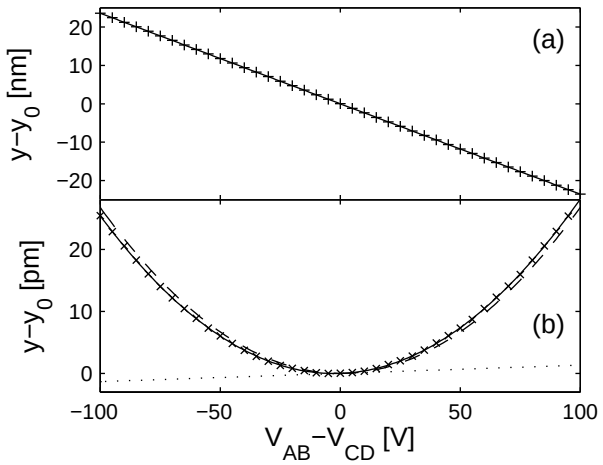

Fig. 5. Thickness change $y - y_0$ in a three-layer structure for (a) bi- and (b) mono-polar charge distributions as a function of the voltage difference between the electrodes $\Delta V = V_{\mathrm{AB}} - V_{\mathrm{CD}}$. The symbols are the values calculated with the FE method. The solid lines (——) are the best linear and quadratic fits. In (b) the fitted curve is separated into its linear (· · · · · ·) and quadratic (– – –) parts, in order to show the electrostrictive and piezoelectric contributions.

the quadratic term, a_{33}^{e} is important indicating 'electrostrictive phenomena'. The calculated deformations for these two systems are shown in Fig. 5. The deformation with the same applied voltage is 1000 times higher for bipolar than for mono-polar charge.

In the simulations, the surface charge densities are $\pm 1\ \mathrm{mC\,m^{-2}}$ and $1\ \mathrm{mC\,m^{-2}}$ for bi- and mono-polar charge distributions. Again, similar to the two-layer system, we first alter the permittivity of the phase a keeping Young's moduli of both phases and the permittivity of the phase b constant. Later, Young's modulus of phase a is varied while all other material parameters are kept constant. The total thicknesses of the phases are equal to each other $x_{\mathsf{a}} = x_{\mathsf{b}}$. There are two different combinations of interest: (i) phase a in Fig. 4 is rigid and the structures is soft-rigid-soft (SRS) or (ii) phase a is soft which leads to a rigid-soft-rigid (RSR) structure. The mono-polar-charge cases do not produce significant electro-mechanical activity comparable to the bipolar ones. Experimental observations performed on some prepared RSR structures, have verified the numerical simulations such that the RSR structures do not yield any observable piezoelectric activity. Moreover, mono-polar-charge samples do not show any measurable electro-mechanical activity.

The results of the simulations are illustrated in Fig. 6. In the figures, the values are normalized respective to a maxima of the absolute parameter values, $\max|a_{33}^{\mathsf{e}}|$, $\max|d_{33}^{\mathsf{e}}|$ and $\max|y_0|$. The normalization values are listed in Table 1 as min and max. In the table, the rigid and soft phase order of the structures are presented together with the parameter that is varied. While the total thickness change behaves differently, the normalized electrostrictive

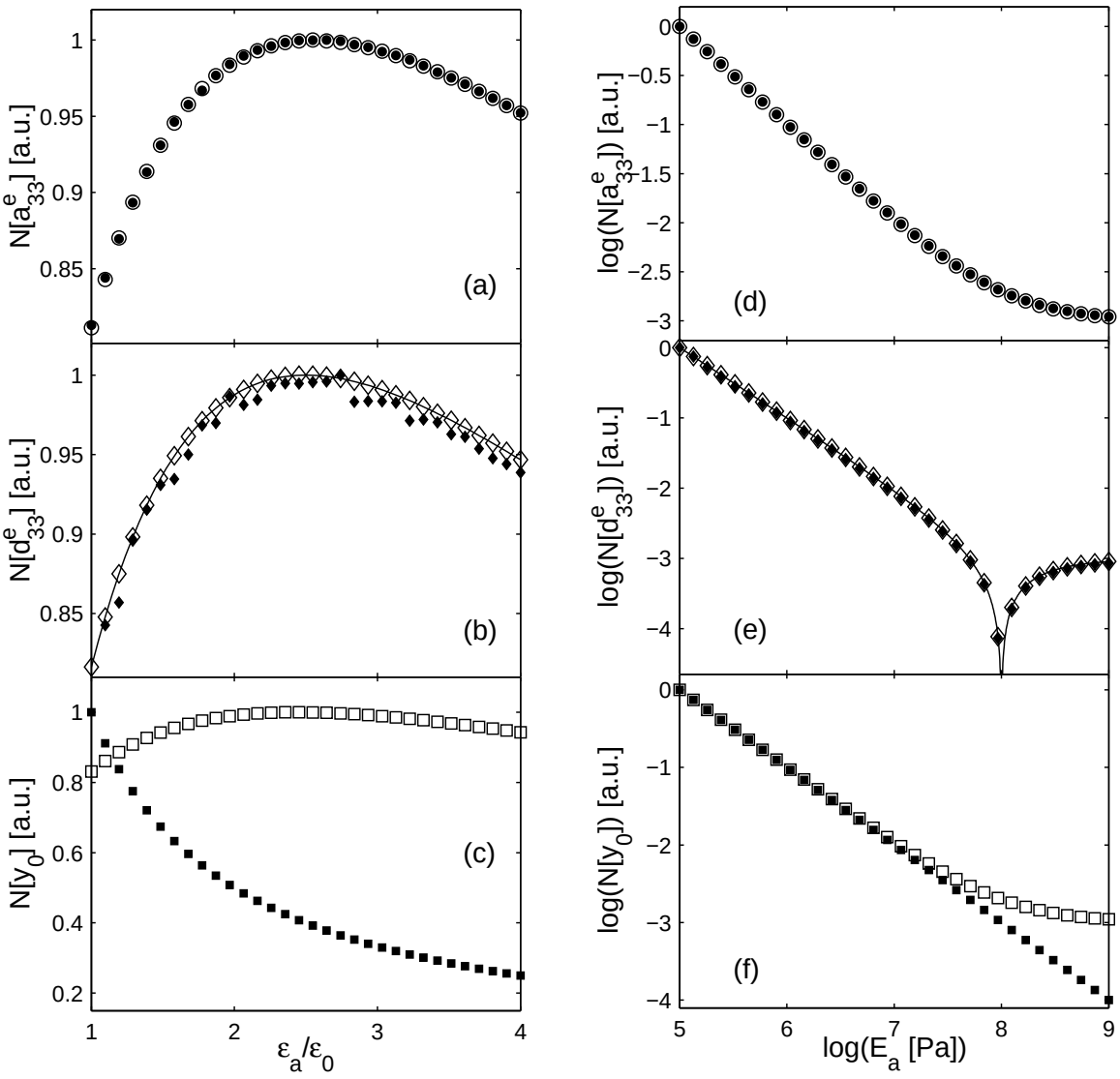

Fig. 6. Calculated (a) electrostriction a^{e}_{33} (b) piezoelectric coefficients d^{e}_{33} and (c) deformation y_0 due to interface charge for altered permittivity of phase a. (d) Electrostriction a^{e}_{33} (e) piezoelectric coefficients d^{e}_{33} and (f) deformation y_0 due to interface charge for altered Young's modulus of phase a. The parameters are normalized with respect to their max or min values, which are presented in Table 1. The filled and empty symbols represent the mono- and bipolar charge cases for the simulations. The solid lines (——) in (b) and (e) are obtained from Eq. (1) with interface charge $\rho = 970$ and 992 $\mu\mathrm{C\,m^{-2}}$, respectively.

and piezoelectric coefficients had the same shape as functions of the relative permittivity of phase a.

In Figs. 6b and 6e, solid lines (——) represent the curve-fitting results obtained with Eq. (1) in which the surface charge ρ is used as a free parameter. It is found that ± 1 mC m^{-2} on the interfaces of a three-layer system yields the same results as a two-layer system with approx. 1 mC m^{-2} at the interface. This is

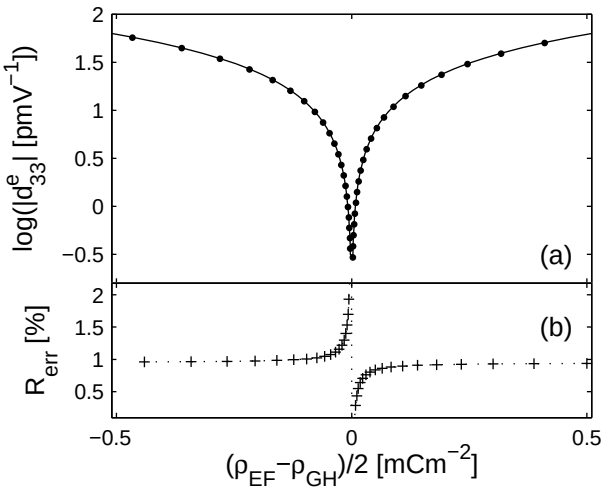

Fig. 7. (a) Calculated piezoelectric coefficient $|d_{33}^{\mathrm{e}}|$ (•) as a function of difference in total charges at boundaries EF and GH. The solid line (——) is Eq. (1) with half the apparent charge. (b) Relative error in percent.

due to the symmetry plane between the two charge layers that can be assumed as in the method of images[27]. Since there is no external field in a three-layer system with bipolar charge–it is neutral–it is to be preferred for non-electrostatic industrial applications. Except for the results of the RSR/ϵ_{a} case, the other three bipolar charge systems result in high piezoelectric coefficients, $d_{33}^{\mathrm{e}} > 200$ pmV^{-1}. It is interesting that the $\max|d_{33}^{\mathrm{e}}|$ and $\min|d_{33}^{\mathrm{e}}|$ values obtained for the RSR/ϵ_{a} and SRS/ϵ_{a} cases are not comparable. The RSR structure is not suitable for any electro-mechanical application. The reason for the very low piezoelectric coefficients in the RSR case is that the structure expands or contracts in response to the internal charge distribution, even in the absence of an applied voltage–y_0 in Table 1. After this deformation there is no (or very little) space for the structure to respond to the applied voltage. It is observed that a d_{33}^{e} value on the order of nmV^{-1} can be obtained if materials with low Young's modulus ($E^{\mathrm{Y}} < 1$ MPa) are employed such as non-conducting polymer foams and natural cork[28].

As mentioned previously, the mono-polar charge systems exhibit very little electro-mechanical activity when the charges at the surfaces are equal. However, at high applied voltages, the electrostrictive effect is significant. To have the same magnitude of the piezoelectric coefficient in a two-layer system one should introduce a surface charge of about 1nC m^{-2} at the interface, which is extremely low. If the surface charges are not equal, but have the same sign, the response of the structure can be tailored to be linear in the applied field for specially selected surface charge values. This is indicated in Fig. 7. When the unbalanced charge of the structure is close to zero, $(\rho_{\mathrm{EF}} - \rho_{\mathrm{GH}})/2 \approx 0$, the analytical solution and the numerical results deviate, due to the numerical error. This is an interesting case, since in phases with significant conductivity,

charges on the surfaces would recombine. This process would directly affect the electro-mechanical activity and lower d_{33}^{e}.

3.3 Two-dimensional system

3.3.1 Non-uniform charge density at the interface

As an illustration for a two-dimensional solution, we again consider a two-layer system as in Fig. 1. However, this time we just alter the charge distribution at the interface EF in the x-direction.

$$\rho(x) = \rho_0 n\pi^{-1}[1 + n^2x^2]^{-1} \tag{10}$$

where n defines the shape of the distribution—for $n \to 0$ surface and $n \to \infty$ line charge distributions are obtained—, and ρ_0 is the charge amplitude. The material properties are taken as $\epsilon_{\mathsf{a}} = \epsilon_{\mathsf{b}} = 2.5$ and $E_{\mathsf{a}}^{\mathrm{Y}} = 1$ MPa and $E_{\mathsf{b}}^{\mathrm{Y}} = 100$ MPa. The boundary conditions are assigned as in the previous problem (see § 3.1). Since the problem is now in two-dimensions the Poisson's ratio of phases ν_{a} and ν_{b} influence the resulting effective piezoelectric coefficient d_{33}^{e}. In Fig. 8a, the results obtained for d_{33}^{e} are illustrated as a function of n for various Poisson's ratios. For small values of n ($n < 10^3$) and $\nu_{\mathsf{a}} = \nu_{\mathsf{b}} \ll 0.1$, d_{33}^{e} is the same as the one-dimensional simulations, a uniform charge distribution. However, as the charge distribution is altered by changing n, the resulting d_{33}^{e} increases for $n > 10^3$ and approaches a constant for $n > 10^4$. These higher values of d_{33}^{e} are expected due to the electric field distribution in the system, which is enhanced at the tip of the charge distribution (sheet-like discontinuous surface charge in the x-direction). The enhancement is higher as the charge distribution approaches a line charge distribution, the piezoelectric coefficient being approx. 10% higher than that of uniform sheet charge distribution. In Fig. 8a and 8b show that d_{33}^{e} decreases with increasing Poisson's ratio, when the latter approaches 0.5.

Finally, as an illustrative example in Fig. 9a the stress distribution and electrical potential are shown. The voltage difference between the AB and CD boundaries is 0 V. The Poisson's ratio of the phases are as follows, $\nu_{\mathsf{a}} = 0.33$ $\nu_{\mathsf{b}} \ll 0.1$. In Fig. 9b the charge distribution at the interface and the deformation on the boundary AB are presented. The deformation is purely due to the interfacial charge, and it is larger than the previous cases considered. The deformation is localized as the charge distribution.

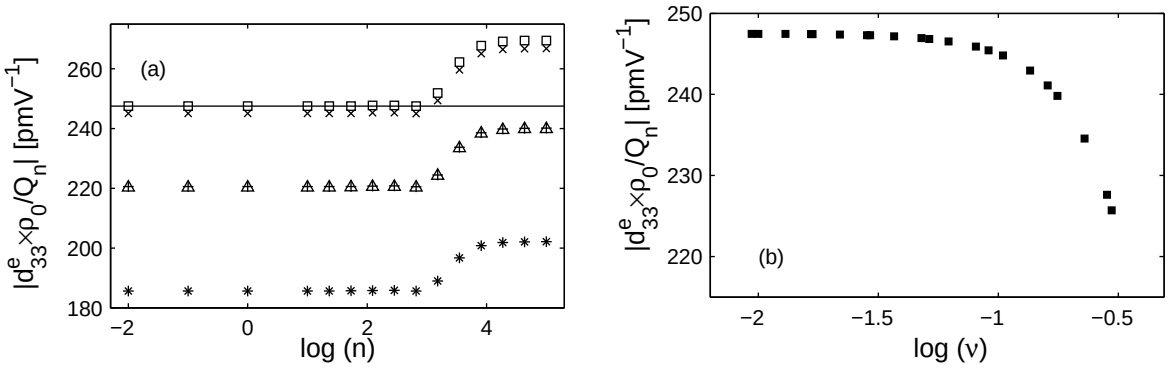

Fig. 8. (a) Calculated absolute values of piezoelectric coefficient $|d^{\mathsf{e}}_{33}|$ normalized to the actual two dimensional charge density $\rho(x)$ for various Poisson's ratio of phases ($\nu = \nu_{\mathsf{a}} = \nu_{\mathsf{b}}$); ($\Box$) $\nu \ll 0.1$, ($\times$) $\nu = 0.1$, ($+$) $\nu = 0.33$, ($*$) $\nu = 0.5$ and ($\triangle$) $\nu_{\mathsf{a}} \ll 0.33$ $\nu_{\mathsf{b}} = 0.1$. The solid line (——) is the value calculated in § 3.1 for uniform surface charge distribution. (b) Influence of Poisson's ratio on d^{e}_{33} for $\nu_{\mathsf{a}} = \nu_{\mathsf{b}} \ll 0.1$.

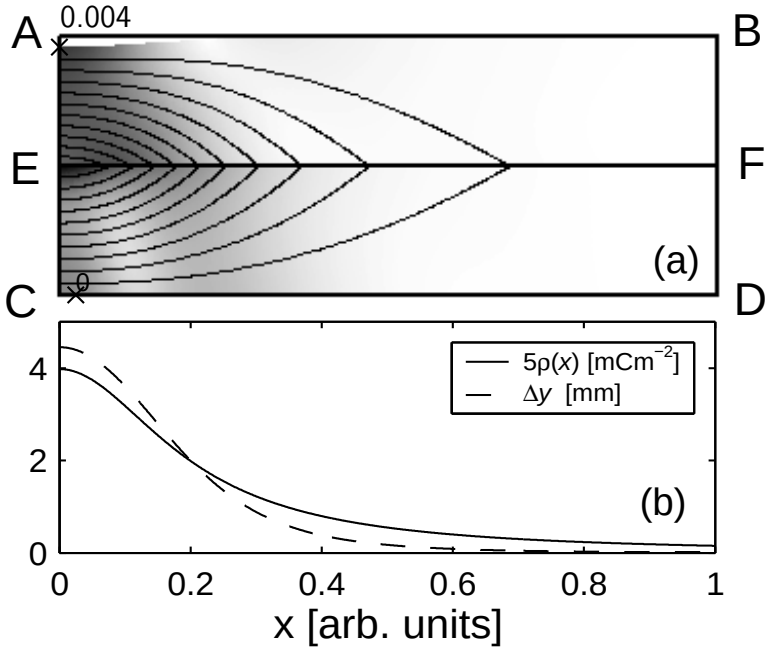

Fig. 9. (a) Mechanical stress (von Mises stress) in gray-scale and voltage distribution in contour plot (for $\Delta V = 0$ V). The structure is deformed, the maximum and minimum deformations are marked with symbols ($\times$), and the values are normalized to thickness of the whole structure, AC. (b) Charge density at the interface EF and deformation of the boundary AB. The charge density is calculated for $n = 10$ and $\rho_0 = 1$ mCm^{-2} in Eq. (10).

3.3.2 Irregularly shape sample

In this section we have considered an irregular shape as illustrated in Fig. 10a. Phase a is considered to be changing its width, |AP|. In the simulation, the

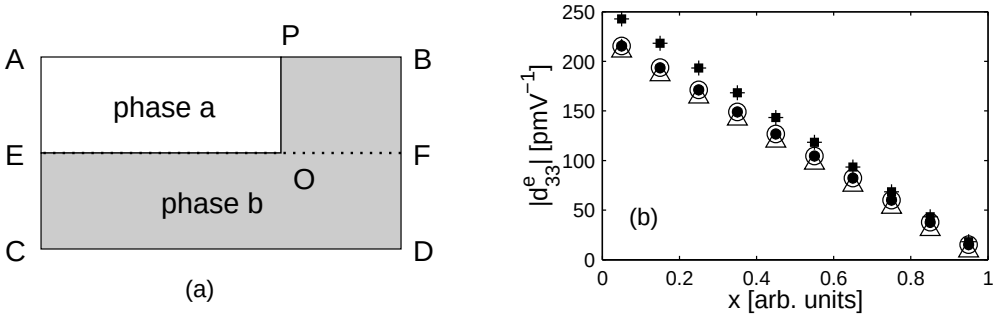

Fig. 10. (a) The geometry used in the calculations for the irregular shape. Phase b is considered to be soft, the length PB is used as a parameter in the calculations, $x = |\mathrm{PB}|/|\mathrm{CD}|$. The dotted line between EF show the charge interface. (b) Calculated absolute values of piezoelectric coefficient $|d^{\mathsf{e}}_{33}|$ for various PB ratio and Poisson' ratio when the charge distribution of 1 mCm^{-2} is considered in the EF interface; (■) $\nu_{\mathsf{a}} = 0.33$ and $\nu_{\mathsf{b}} \ll 0.1$, (+) $\nu_{\mathsf{a}} \ll 0.1$ and $\nu_{\mathsf{b}} \ll 0.1$, (•) $\nu_{\mathsf{a}} \ll 0.1$ and $\nu_{\mathsf{b}} = 0.33$, (▽) $\nu_{\mathsf{a}} = 0.33$ and $\nu_{\mathsf{b}} = 0.33$, (○) $\nu_{\mathsf{a}} = 0.5$ and $\nu_{\mathsf{b}} = 0.33$. When only charge is considered in the EO the piezoelectric coefficient is not altered significantly, (△) $\nu_{\mathsf{a}} = 0.5$ and $\nu_{\mathsf{b}} = 0.33$.

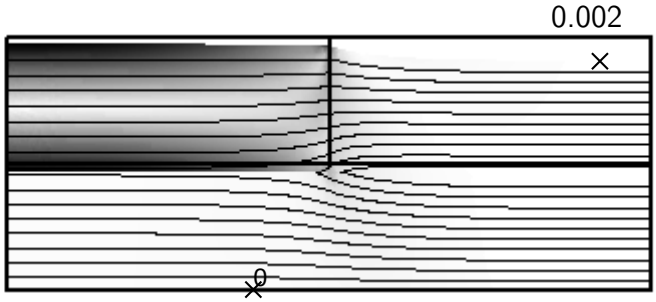

Fig. 11. Mechanical stress (von Mises stress) in gray-scale and voltage distribution in contour plot (for $\Delta V = 0$ V). The structure is deformed, the maximum and minimum deformations are marked with symbols (×), and the values are normalized to the thickness of the whole structure, AC. The Poisson's ratio of phase a is 0.33.

same consideration as in the previous cases are considered, $\epsilon_{\mathsf{a}} = \epsilon_{\mathsf{b}} = 2.5$ and $E^{\mathrm{Y}}_{\mathsf{a}} = 1$ MPa and $E^{\mathrm{Y}}_{\mathsf{b}} = 100$ MPa. The charge is assumed to be on the interface EF with the charge density 1 mCm^{-2}. The results are plotted in Fig. 10b for various Poisson's ratio of phases and fraction of phase a, $1 - x$ where x is the length of PB. It is clear that the Poisson's ratio of the soft phase (phase b) influences the piezoelectric coefficient $|d^{\mathsf{e}}_{33}|$. Moreover, as the fraction of the rigid phase is lowered, $x \to 0$, the piezoelectric activity is decreasing linearly with the fraction of phase b, which is expected. In addition the decrease in d^{e}_{33} with respect to x is proportional to the Poisson's ratio of phase b. In Fig. 11 the stress and the electric potential distributions are presented as gray-scale and contour plots.

4 Conclusions

Numerical simulations on the electro-mechanical properties of layered structures containing charges are reported. The simulations take the coupling of the electrical and mechanical stresses into account by means of *the Maxwell stress tensor*. The results are compared with an analytical model, and it is observed that there is good agreement for two-layer systems. The piezoelectricity in three-layer systems shows a strong dependence on the polarity of interface charges. It is concluded that bipolar charge systems clearly yield higher piezoelectric coefficient values than mono-polar charge systems. The mono-polar charge cases are dominated by 'electrostrictive effects'.

In this paper, we have presented a way of calculating electro-mechanical activity of layered electrets with uniform and non-uniform charge distributions. The numerical model is also applied to a two-layer system with discontinuous interface charge layer. In such a simulation unlike the one-dimensional calculations the Poisson's ratio of the phases become significant. High Poisson's ratio lead to low the electro-mechanical coefficient. As the sheet of charge at the interface is modified toward a line charge distribution the piezoelectric coefficient is increased approx. 10%. The two-dimensional structures considered have also illustrated the stress distribution in the constituents are of importance, the stiff phase is mechanically stressed due to electromechanical activity in the soft phase. We might conclude that the presence of excess charges (space charge) in heterogeneous systems is crucial for aging of the materials.

As a concluding remark, it is illustrated that in heterogeneous materials, fluctuations in the local electric field could lead to mechanical deformations even if there is no intrinsic piezoelectricity in the phases. The considered cases show that the deformation follows the actual charge distribution at the interface, and distribution of charges plays an important role in materials with irregularity.

References

[1] R. Gerhard-Multhaupt. Less can be more. holes in polymers lead to a new paradigm of piezoelectric materials for electret transducers. *IEEE Transactions on Dielectrics and Electrical Insulation*, 9(5):850–859, 2002.

[2] S. Bauer, R. Gerhard-Multhaupt, and G. M. Sessler. Ferroelectrets: Soft electro active foams for transducers. *Physics Today*, pages 37–43, February 2004.

[3] W. G. Cady. *Piezoelectricity: An introduction to the theory and applications of electrical phenomena in crystals.* Dover Publications Inc., New York, new revised edition, 1964.

[4] G. Dreyfus and J. Lewiner. Free energy of electrets. *Physical Review B*, 14(12):5451–5457, 1976.

[5] H. J. Wintle and R. Dörsam. Phenomenological piezoelectricity of polymer insulators. *Physical Review B*, 39(6):3862–3870, 1989.

[6] R. Kacprzyk, E. Motyl, J. B. Gajewski, and A. Pasternak. Piezoelectric properties of nonuniform electrets. *Journal of Electrostatics*, 35:161–166, 1995.

[7] M. Paajanen, H. Välimäki, and J. Lekkala. Modelling the electromechanical film (EMFi). *Journal of Electrostatics*, 48:193–204, 2000.

[8] R. Gerhard-Multhaupt, W. Künstler, T. Görne, A. Pucher, T. Weinhold, M. Seiß, Zhongfu Xia, A. Wedel, and R. Danz. Porous PTFE space-charge electrets for piezoelectric applications. *IEEE Transactions on Dielectrics and Electrical Insulation*, 7(4):480–492, 2000.

[9] W. Künstler, Z. Xia, T. Weinhold, A. Pucher, and R. Gerhard-Multhaupt. Piezoelectricity of porous polytetrafluoroethylene single- and multi-film electrets containing high charge densities of both polarities. *Applied Physics A*, 70:5–8, 2000.

[10] G. M. Sessler and J. Hillenbrand. Electromechanical response of cellular electret films. *Applied Physics Letters*, 75(21):3405–3407, 1999.

[11] M. Lindner, S. Bauer-Gogonea, S. Bauer, M. Paajanen, and J. Raukola. Dielectric barrier microdischarges: Mechanisims for charging of cellular piezoelectric polymers. *Journal of Applied Physics*, 91(8):5283–5287, 2002.

[12] R. Schwödiauer, G. S. Neugschwandtner, K. Schrattbauer, M. Lindner, M. Vieytes, S. Bauer-Gogonea, and S. Bauer. Prepareation and characterization of noval piezoelectric and pyroelectric polymer electrets. *IEEE Transactions on Dielectrics and Electrical Insulation*, 7(4):578–586, 2000.

[13] M. Paajanen, J. Lekkala, and K. Kirjavainen. Electromechanical film EMFi-a new multipurpose electret material. *Sensors and Actuators A: Physical*, 84:95–102, 2000.

[14] M. Paajanen, J. Lekkala, and H. Välimäki. Electromechanical modeling and properties of the electret film EMFi. *IEEE Transactions on Dielectrics and Electrical Insulation*, 8(4):629–636, 2001.

[15] S. Torquato. *Random Heterogeneous Materials: Microstructure and macroscopic properties*, volume 16. Springer-Verlag, Berlin, 2001.

[16] E. Tuncer, S. M. Gubański, and B. Nettelblad. Non-debye dielectric relaxation in binary dielectric mixtures (50-50): Randomness and regularity in mixture topology. *Journal of Applied Physics*, 92(8):4612–4624, 2002.

[17] E. Tuncer, Y. V. Serdyuk, and S. M. Gubanski. Dielectric mixtures: electrical properties and modeling. *IEEE Transactions on Dielectrics and Electrical Insulation*, 9(5):809–828, 2002.

[18] O. Sigmund, S. Torquato, and I. A. Aksay. On the design of 1-3 piezocomposites using topology optimization. *Journal of Materials Research*, 13(4):1038–1048, 1998.

[19] L.D. Landau and E.M. Lifshitz. *Electrodynamics of continuous media*,

volume 8 of *Course of Theoretical Physics*. Perganom Press, New York, 2nd edition, 1982.

[20] FEMLAB *Electromagnetics Module*. Comsol AB, Stockholm, Sweden, 2.3 edition, 2002.

[21] R. Gerhard-Multhaupt. Analysis of pressure-wave methods for the non-destructive determination of spatial charge or field distribution in dielectrics. *Physical Review B*, 27(4):2494–2503, 1983.

[22] O. Paris, J. Lewiner, T. Ditchi, S. Holé, and C. Alquié. A finite element method for the determination of space charge distributions in complex geometry. *IEEE Transactions on Dielectrics and Electrical Insulation*, 7 (4):556–560, 2000.

[23] FEMLAB *User's Guide and Introduction*. Comsol AB, Stockholm, Sweden, 2.2 edition, 2001.

[24] G. S. Neugschwandtner, R. Schwödiauer, S. Bauer-Gogonea, and S. Bauer. Large piezoelectric effects in charged, heterogeneous fluoropolymer electrets. *Applied Physics A*, 70:1–4, 2000.

[25] Matweb: Material property data. Automation Creations, Inc., Christiansburg, VA USA: `http://www.matweb.com`, 2003.

[26] E. Butkov. *Mathematical Physics*. Addison-Wesley Series in Advanced Physics. Addison-Wesley Publishing Company, Menlo Park, 1968.

[27] L. Eyges. *The Classical Electromagnetic Field*. Dover, New York, 1972.

[28] M. F. Ashby and Kara Johnson. *Materials and Design: The Art and Science of Materials Selection in Product Design*. Butterworth Heinemann, Oxford, 2002.

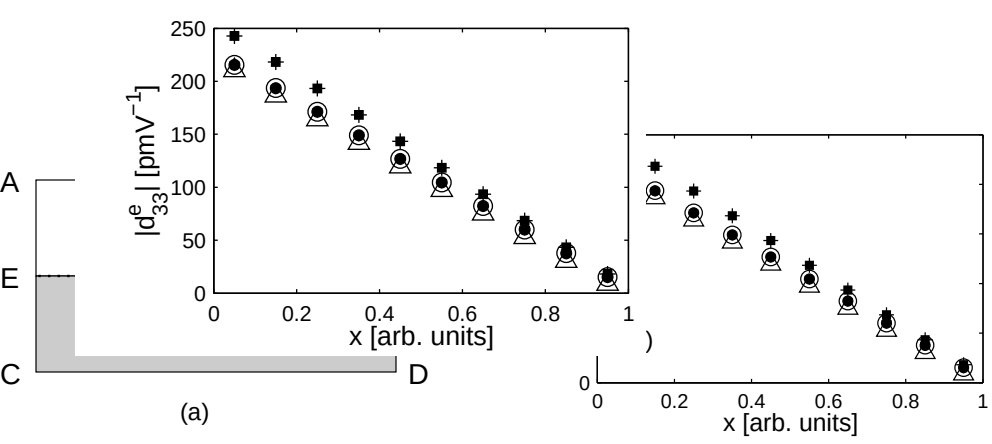
A
E
C
D
250
200
150
100
50
0
0
0.2
0.4
0.6
0.8
1
x [arb. units]
$|d^e_{33}|$ [pmV^{-1}]
0
0.2
0.4
0.6
0.8
1
x [arb. units]

(a)

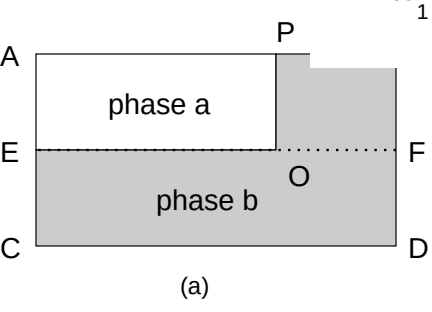
P
A
phase a
E
F
O
phase b
C
D

(a)

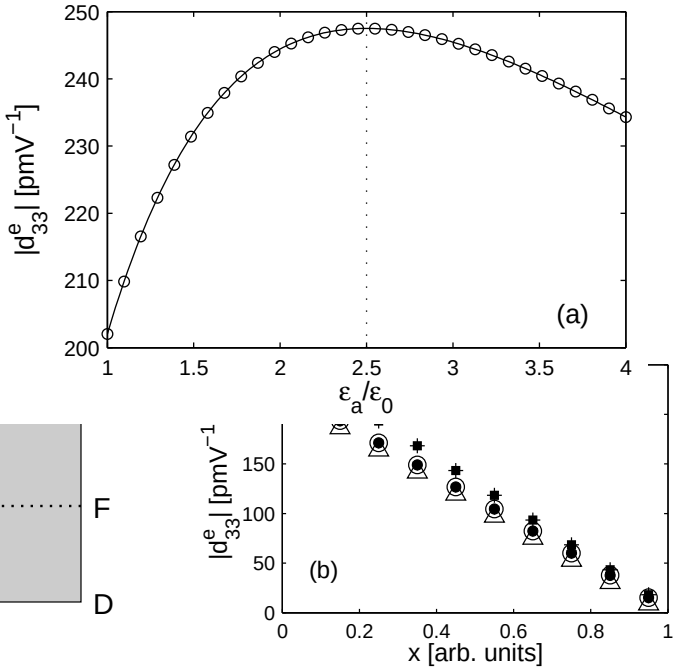
250
240
230
220
210
200
1
1.5
2
2.5
3
3.5
4
$|d^e_{33}|$ [pmV^{-1}]
$\varepsilon_a/\varepsilon_0$
(a)
150
100
50
0
0.2
0.4
0.6
0.8
1
x [arb. units]
(b)

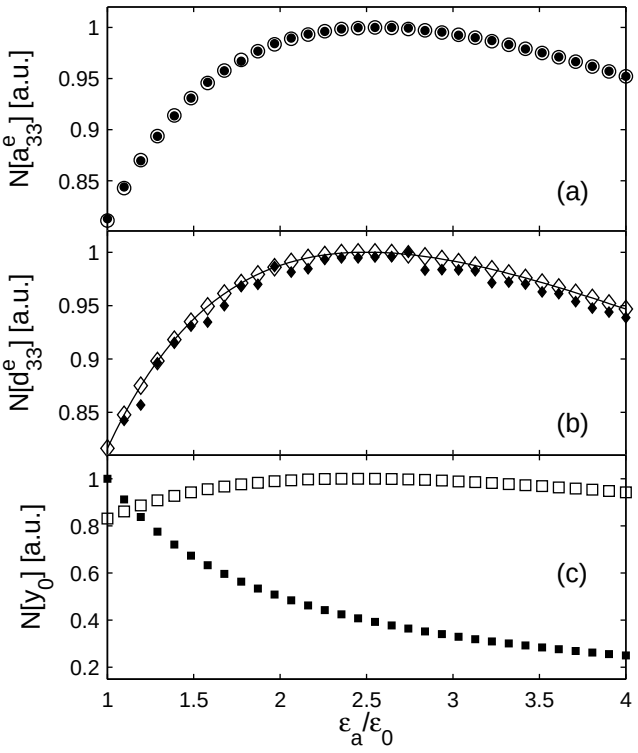
N[a^e_33] [a.u.]
N[d^e_33] [a.u.]
N[y_0] [a.u.]
(a)
(b)
(c)
1
0.95
0.9
0.85
0.8
0.6
0.4
0.2
1
1.5
2
2.5
3
3.5
4
ε_a/ε_0

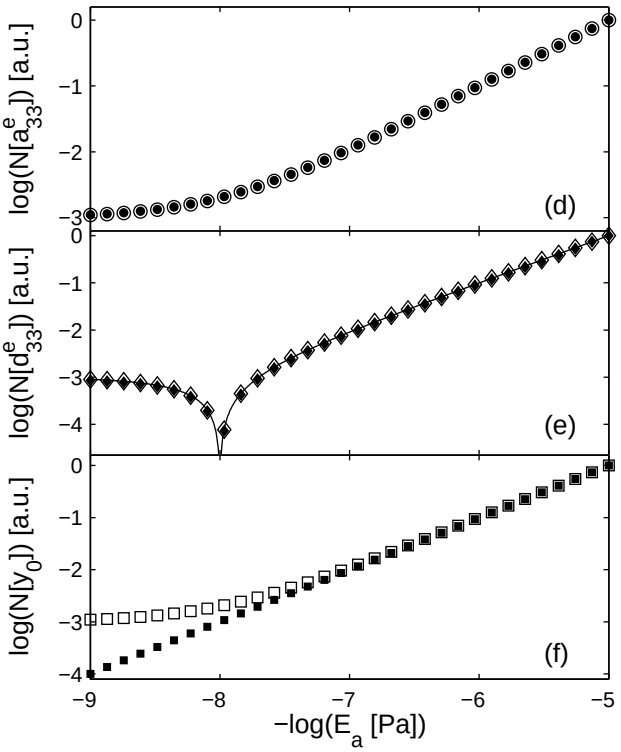
log(N[a$^e_{33}$]) [a.u.]
log(N[d$^e_{33}$]) [a.u.]
log(N[y$_0$]) [a.u.]
(d)
(e)
(f)
0
−1
−2
−3
−4
−9
−8
−7
−6
−5
−log(E$_a$ [Pa])

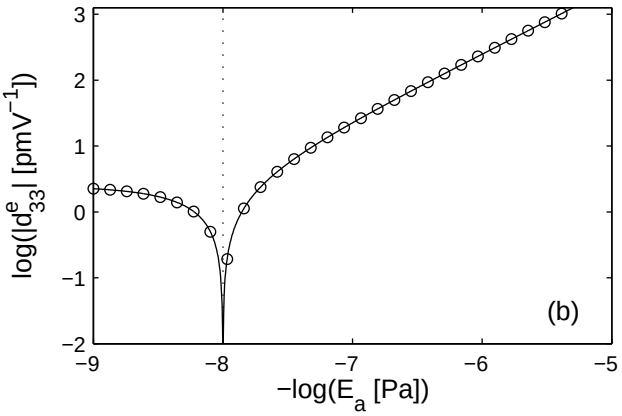
3
2
1
0
−1
−2
−9
−8
−7
−6
−5
log(|d$^e_{33}$| [pmV^{-1}])
−log(E$_a$ [Pa])
(b)